Volume 41 | Number 21 | 7 November 2017 | Pages 12339–13184

NJC

New Journal of Chemistry

A journal for new directions in chemistry

rsc.li/njc

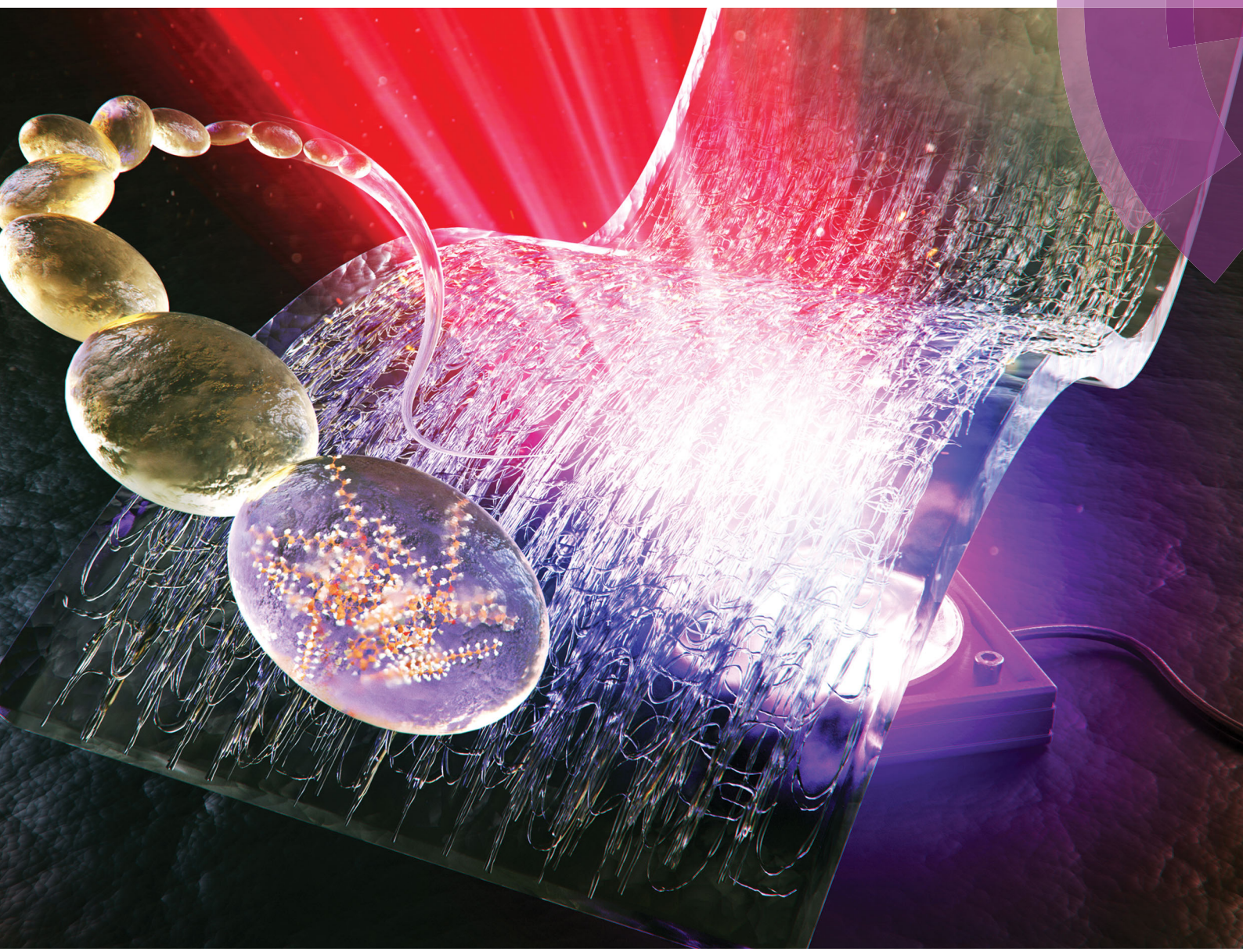

ISSN 1144-0546

ROYAL SOCIETY OF CHEMISTRY

LETTER

Hyungwoo Kim, Ji Young Chang *et al.*

A versatile platform for lanthanide(III)-containing organogelators: fabrication of the Er(III)-incorporated polymer nanocomposite from an organogel template

cnrs

NJC

PAPER

Cite this: *New J. Chem.*, 2017, **41**, 13140

Two isomeric solid carbon nitrides with 1 : 1 stoichiometry which exhibit strong mechanical anisotropy†

Sergey V. Bondarchuk *[a] and Boris F. Minaev[ab]

Received 25th January 2017,
Accepted 25th September 2017

DOI: 10.1039/c7nj00316a

rsc.li/njc

Two isomeric layered carbon nitride phases in a trigonal crystal system with 1 : 1 stoichiometry, **NCCN** and **NCNC** (space group *P*3*m*1), are studied using first principles calculations and quantum theory of atoms in molecules (QTAIM) analysis, where the latter phase is predicted for the first time. Comprehensive characterization of these materials is performed to determine their thermodynamic, elastic and spectral (vibrational, UV-vis and NMR) properties. High-throughput scheme for band structure calculations along with the accurate hybrid functional HSE06 provide the indirect band gaps of 3.142 eV (**NCNC**) and 5.021 eV (**NCCN**). Phonon dispersion calculations prove that the studied materials are dynamically stable at ambient pressure. The **NCCN** phase demonstrates a poor spectral pattern on infrared (IR) intensities and Raman activities, whereas the **NCNC** polymorph is expected to be effectively detectable by both spectral techniques. The UV-vis spectra of the studied phases display absorption bands between *ca.* 50–150 nm, which indicates that these isomers are transparent to visible light. Elastic constant calculations indicate strong anisotropy of their Young's moduli. In the [1 0 0] ≡ [0 1 0] plane directions the modulus values are 914.6 GPa (**NCNC**) and 865.1 GPa (**NCCN**). In the [0 0 1] direction, which is perpendicular to the layer plane, the Young's moduli are much smaller and equal to 73.3 GPa and 58.4 GPa for **NCNC** and **NCCN**, respectively. The exfoliation energies are expected to be about 3 (**NCNC**) and 2 (**NCCN**) times higher than those of graphite.

Introduction

Carbon–nitride structures, as molecular tandems, have attracted increasing interest due to their remarkable physical and chemical properties. When combined together, nitrogen and carbon atoms eliminate the drawbacks of their own allotropes, such as the ambient pressure metastability of solid nitrogen phases (cubic gauche or trigonal)[1,2] or inappropriate electronic structure of graphene for applications in nanoelectronics and photonics.[3] An excellent example of such synergism is a layered CN allotrope, namely, graphitic carbon nitride (g-C_3N_4). The recent advanced applications of g-C_3N_4 include photocatalysis,[4–10] enhanced oxygen reduction,[11–13] methanol oxidation,[14] sodium[15] and lithium-ion batteries,[16] hydrogen storage,[17,18] electrochemical determination of mercury[19] and spintronics.[20]

The search for novel solids harder than diamond and with low compressibility has resulted in theoretical prediction of new carbon nitride phases. Liu and Cohen first successfully predicted the β-C_3N_4 polymorph (space group *P*3) in 1989.[21] In addition to β-C_3N_4, Teter and Hemley in 1996 predicted four novel polymorphs, namely, α-C_3N_4 (space group *P*31*c*), cubic-C_3N_4 (space group $I\bar{4}3d$), pseudocubic-C_3N_4 (space group $P\bar{4}2m$) and g-C_3N_4 (space group $P\bar{6}m2$).[22] Further theoretical investigations of the electronic,[23] vibrational and dielectric properties of C_3N_4 polymorphs[24] should be mentioned in addition to studying their stability,[25] nature of space group for g-C_3N_4,[26] the effect of nitrogen vacancies[27] and spin transport properties.[28] In addition to the C_3N_4 composition, a thermodynamic analysis of the C_4N_3 carbon nitride formation was also reported.[29]

Compounds with a 1 : 1 stoichiometry play a crucial role in the large family of different C_xN_y polymorphs. The intense search and study of such solid phases started after the seminal paper by Côté and Cohen in 1997, who studied eight different structures, namely those of rocksalt (RS), zinc-blende (ZB), GeP, rhombohedral, H-6, bct-4, β-InS, and GaSe crystals. It was determined that for this stoichiometry the sp^2 bonding of

[a] *Department of Chemistry and Nanomaterials Science, Bogdan Khmelnitsky Cherkasy National University, blvd. Shevchenko 81, 18031 Cherkasy, Ukraine. E-mail: bondchem@cdu.edu.ua*
[b] *Division of Theoretical Chemistry and Biology, School of Biotechnology, KTH Royal Institute of Technology, 10691 Stockholm, Sweden*

† Electronic supplementary information (ESI) available: Graphical description of the vibrational modes, optical and thermodynamic properties, elastic stiffness and compliance constants, and also QTAIM parameters. See DOI: 10.1039/c7nj00316a

nitrogen is energetically preferable to sp^3.[30] However, further studies revealed that this is not the case.[31,32] The GaSe phase has a structural motif very close to the **NCCN** (*P*3*m*1) phase. Furthermore, it was found that cubic-to-tetragonal phase transitions, namely, ZB to β-tin, bcc to bct, and RS to tetragonal RS (tet-RS) are energetically preferable.[33]

Later on, Wang predicted eight sp^3-hybridized polymorphs of C_1N_1 (including the previously found cg-NC phase[34]) using the particle swarm optimization (PSO) algorithm.[32] These polymorphs include the following space groups: *P*4/*mnc*, $P4_2/mnm$, *Aea*2, *Pnnm*, *Pbam*, *P*6/*m* and $P\bar{3}m1$. It should be noted that the $P\bar{3}m1$ phase is very structurally similar to the previously predicted GaSe form.[30] The $P\bar{3}m1$ phase is an analogue to the **NCCN** phase reported herein. The energy difference between the $P\bar{3}m1$ and *P*3*m*1 space group representation is negligible. It was found that the most energetically favorable phase is β-InS (*Pnnm*), while the (GaSe) $P\bar{3}m1$ polymorph is the next most stable phase.[32,35] To the best of our knowledge, to date, the most energetically favorable polymorph of C_1N_1 is the tetragonal $P4_2/m$ phase, which is more stable than the β-InS phase by about 0.05 eV per f.u.[36] Although a number of different C_xN_y polymorphs have been theoretically simulated, the synthesis of the C_3N_4 phase other than g-C_3N_4 remains elusive. However, the synthesis of the highly incompressible C_1N_1 compound of the *Pnnm* space group has been recently reported.[37]

In addition to the aforementioned crystal solid CN structures, there is an amorphous form of carbon nitride.[38,39] This amorphous form appears after the removal of a nitrogen atom from the C_3N_4 phase and subsequent cell relaxation.[28] Naturally, the bulk modulus of the amorphous form is much lower than that of solid C_3N_4.[28] In contrast, replacement of a carbon atom by nitrogen is widely studied for fullerenes,[40–42] carbon nanotubes,[43–46] CN clusters,[47,48] half-metallic hydrogenated g-C_3N_4[49] and high-energy density materials.[50]

Taking into account the wide applicability of 3D and 2D carbon–nitrogen structures, we tried to find and comprehensively describe some new layered CN materials with 1 : 1 stoichiometry. As a result, a new carbon nitride phase (**NCNC**) is predicted and characterized and also compared with its known isomeric form (**NCCN**) whose properties are not described in the literature.[32] In addition, these polymorphs are among the most thermodynamically stable phases. Moreover, the layered character of **NCNC** and **NCCN** allows the formation of the corresponding 2D structures, which have their own interesting properties.

Computational details

The Cambridge Serial Total Energy Package (CASTEP) code[51] implemented in the Materials Studio 7.0 suite of programs[52] was applied for the first principles calculations of equilibrium geometries, and spectral, thermodynamic and mechanical properties presented in this study. The calculations were carried out within the generalized gradient approximation (GGA). A norm-conserving pseudopotential (NCP) in reciprocal space was used entirely to describe the electron-core interactions.

For cell relaxation and phonon calculations, we used the density functional parameterized by Perdew–Burke–Ernzerhof (PBE),[53] whereas for the mechanical properties calculations, the modified functional, namely, PBE for solids (PBEsol)[54] was applied. At the same time, for band structure calculations we utilized a set of different pure and hybrid GGA functionals. In addition to the aforementioned pure functionals, we also used the functional developed by Perdew and Wang (PW91).[55] Among the available hybrid functionals, we used the most popular ones, namely, PBE0,[56] B3LYP,[57] and HSE06.[58] The latter functional was recently proven to produce band gaps, which are close to the experimentally obtained ones.[59] The electronic wave functions were expanded in a plane wave basis set with an energy cutoff of 1000 eV (73.5 Ry). The Monkhorst–Pack *k*-point sampling scheme with a 16 × 16 × 6 (0.03 $Å^{-1}$) *k*-point mesh was specified during all calculations and the SCF tolerance was set to 1×10^{-6} eV per atom.

For the GGA/PBE approach, long-range correlations were taken into account using the Tkatchenko–Scheffler (TS) scheme,[60] whereas for the GGA/PW91 approximation the dispersion correction by Ortmann–Bechstedt–Schmidt (OBS)[61] was applied entirely. The PBE-TS energies are proven to be reliable.[62] The phonon dispersion calculation was carried out using the finite displacement method. The latter provides reliable results even when Vanderbilt type pseudopotentials are used.[63] Molecular visualizations were performed using the Virtual NanoLab 2016.3 program package.[64] The cohesive energy was calculated as follows:

$$E_{coh} = -(E_{phase} - (2E_N + 2E_C))/4 \quad (1)$$

where E_{phase} is the total enthalpy (PBE-TS) of the **NCNC** or **NCCN** phase; and E_N and E_C are the total enthalpies of an isolated nitrogen and carbon atom, respectively; these were obtained in terms of the supercell approximation (vacuum slab thickness of 15 Å). Finally, the Quantum Theory of Atoms in Molecules (QTAIM) analysis of the critical points (CPs) in the **NCNC** and **NCCN** phases was performed using the Critic2 software.[65] To perform the QTAIM analysis, wavefunctions were obtained using the projector augmented wave based method (PAW).[66] This calculation was performed using the Quantum Espresso 4.3.2 program package.[67]

Results and discussion

Structure and electronic properties

The optimized asymmetric cells of the **NCNC** and **NCCN** polymorphs are illustrated in Fig. 1a and b and the alignment of the layers is presented in Fig. 1c. Geometry optimization with complete cell relaxation led to trigonal crystal systems of the $\bar{3}m$ Laue class and *P*3*m*1 space group (Fig. 1). Our structural results for the **NCCN** phase are in a good agreement with those previously reported by Wang *et al.*[32] At 10 GPa the lattice parameters are as follows (our results are presented in parentheses): a = 2.3736 (2.3773) Å and c = 5.3481 (5.2796) Å.[32] At 0 GPa pressure

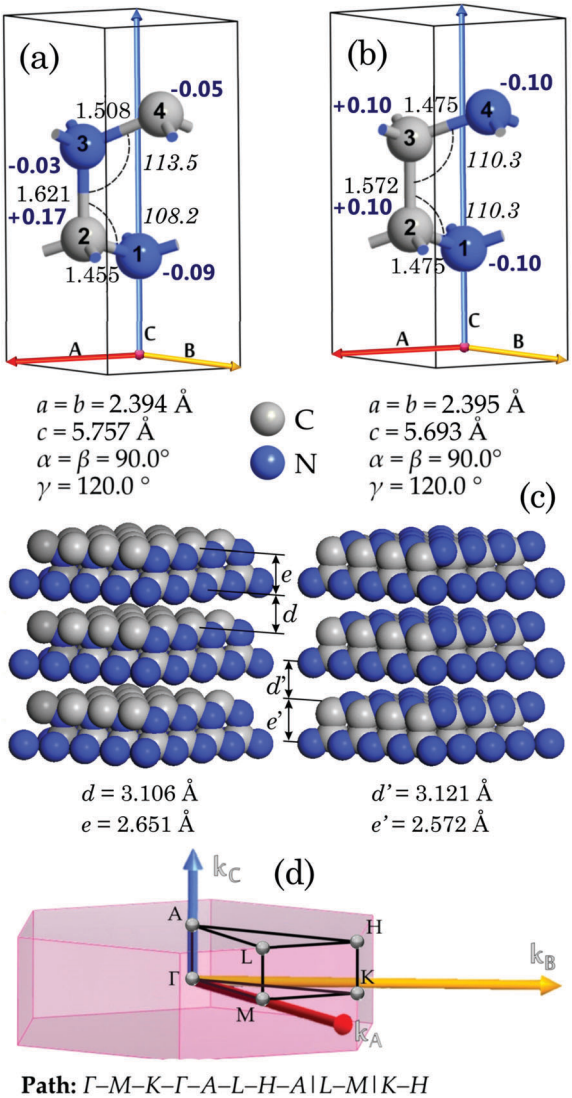

Fig. 1 Optimized asymmetric cell parameters for the **NCNC** (a) and **NCCN** (b) phases; crystal packing and layer spacing (c) and the corresponding Brillouin zone path (d).

the interlayer distance in the **NCCN** phase is 3.121 Å. The new polymorph **NCNC** possesses similar layer spacings, where the gap between the layers is 3.106 Å (Fig. 1c). At zero external pressure the cell volumes are equal to 28.57 (**NCNC**) and 28.28 Å^3 (**NCCN**). Thus, the crystal densities are 3.03 (**NCNC**) and 3.06 (**NCCN**) g cm^{-3}.

The predicted new phase **NCNC** lies 2.296 eV higher in energy than the isomeric **NCCN** phase. This energy difference slightly increases in pressure up to 100 GPa, where it reaches the value of 2.582 eV. In the studied crystals, the atoms occupy the following Wyckoff positions: atoms 1 (1a), atoms 2 and 3 (1c) and atoms 4 (1b). Thus, the fractional coordinates are **NCNC**: N1 (0, 0, 0.234); C2 (2/3, 1/3, 0.327), N3 (2/3, 1/3, 0.661) and C4 (1/3, 2/3, 0.779) and **NCCN**: N1 (0, 0, 0.225); C2 (2/3, 1/3, 1/3), C3 (2/3, 1/3, 2/3) and N4 (1/3, 2/3, 0.775). The most important resonance structures of the studied carbon nitride polymorphs are illustrated in Scheme 1. It is clear that the **NCNC** phase is more stabilized by resonance and delocalization.

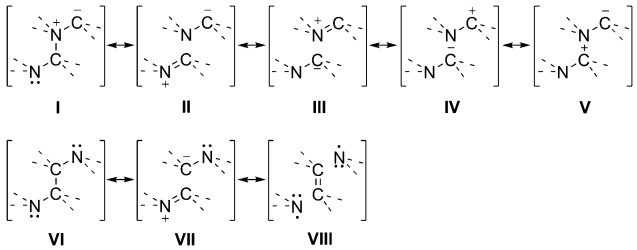

Scheme 1 The most relevant resonance structures for the studied carbon nitride polymorphs.

According to the analysis of the bond lengths and Hirshfeld atomic charges (bold numbers in Fig. 1a and b), the most relevant resonance structures for **NCNC** and **NCCN** are structures V and VI, respectively (Scheme 1).

In order to study the electronic properties of the **NCNC** and **NCCN** polymorphs, we performed band structure (BS) calculations. As mentioned above, we carried out a series of BS calculations using both the pure GGA and hybrid functionals. Since hybrid functionals require a very long time to perform the calculations, we earlier determined a minimal approach that allows the reproduction of stable results.[2] This includes a minimum cutoff energy of 700 eV and a 4 × 4 × 4 *k*-point sampling mesh. Furthermore, the BS calculations were performed in terms of the high-throughput approach, which includes a standard definition of the high symmetry *k*-path for all 14 Bravais lattices and their 24 Brillouin zones.[68] In the case of the hexagonal lattice type, the coordinates of the high-symmetry *k*-points are listed in Table 1 and the corresponding Brillouin zone integration path is illustrated in Fig. 1d.

The results of the BS calculations, obtained using the NCP/700 eV approach with different functionals, are collected in Table 2. As can be seen in Table 2, the pure GGA functionals significantly underestimate the band gap (E_g) values compared to the results from hybrid functionals. We support the previously obtained conclusion that the HSE06 functional provides E_g values close to the experimental values.[59] Thus, the band gaps of **NCNC** and **NCCN** are 3.142 and 5.021 eV (Table 2). We should stress that all the applied methods provide a similar trend for the estimation of E_g. The correlation between the E_g values for **NCNC** and **NCCN** gives R^2 = 0.999.

Table 1 Definition of high symmetry *k*-points in the hexagonal lattice type

k	$\times k_A$	$\times k_B$	$\times k_C$	*k*	$\times k_A$	$\times k_B$	$\times k_C$
Γ	0	0	0	*K*	1/3	1/3	0
A	0	0	1/2	*L*	1/2	0	1/2
H	1/3	1/3	1/2	*M*	1/2	0	0

Table 2 The band gap values calculated using different pure GGA and hybrid functionals with a 700 eV energy cutoff

Phase	PBE	PBEsol	PW91	PBE0	B3LYP	HSE06
NCNC	1.948	1.819	1.978	3.935	3.677	3.142
NCCN	3.638	3.465	3.676	5.819	5.639	5.021

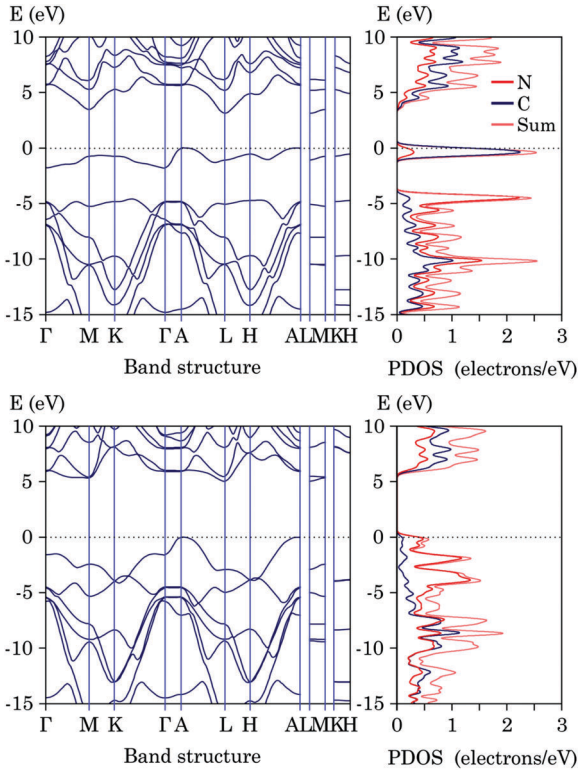

Fig. 2 Band structure and partial density of states (PDOS) for the **NCNC** (top) and **NCCN** (bottom) polymorphs calculated using the NCP/HSE06/700 eV approach.

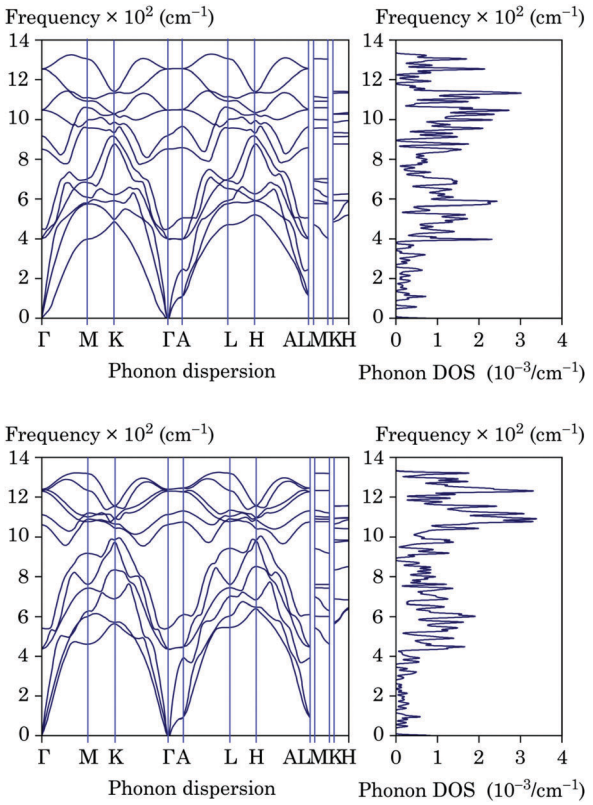

Fig. 3 Zero external pressure phonon dispersion and density of phonon states for the **NCNC** (top) and **NCCN** (bottom) polymorphs.

The BS plots obtained using the NCP/HSE06/700 eV approach are illustrated in Fig. 2. As seen in Fig. 2, the difference between E_g is 1.879 eV (GGA/HSE06). The reason for this difference is the delocalized nature of **NCNC**. Remarkably, the BS plot of the **NCNC** phase demonstrates a rather flat valence band, which does not overlap with the deeper bands. The analysis of PDOS revealed that the 2p-C states provide the main contribution to the valence band (Fig. 2 and Fig. S1 in the ESI†). Each C4 atom bears a lone pair on an sp^3 hybridized orbital forming a non-bonding type valence band. In the case of the localized structure of **NCCN**, such effect does not appear and the valence and conduction bands are split much more.

Phase stability and spectral pattern

Although the **NCCN** polymorph is already known,[32] its dynamic stability has not been determined. A structurally close polymorph, namely GeSe, was found to be dynamically unstable at ambient pressure.[34] Thus, it becomes very important to estimate the dynamic stability of the two predicted materials: the new polymorph (**NCNC**) and its known isomeric form (**NCCN**). For this purpose, we performed phonon dispersion calculations for both the crystals, and the obtained plots are illustrated in Fig. 3. Noteworthy, the phonon spectra are characterized by the absence of soft modes. Upon an applied external pressure, the studied carbon nitride polymorphs conserve dynamic stability up to 200 GPa. Around the Γ-point, the acoustic branches remain linear in both the phases. Moreover, in the case of both polymorphs, degeneracy of two branches takes place (Fig. 3), which assumes equal sound velocity values.

Moreover, we calculated the infrared (IR) intensities and Raman activities at the Γ-point. The asymmetric cells of the studied carbon nitrides contain four atoms, which give rise to a total of twelve modes, in which nine modes are optical. The calculated spectral data are listed in Table 3. As can be seen in Table 3, the vibrational spectra consist of three doubly-degenerate modes and three single modes. The frequencies of the analogous vibrations in the studied polymorphs differ from each other. The stronger bonds have higher force constants, which affect the frequency values. Due to symmetry constraints, the IR spectrum of **NCCN** has very poor pattern of intensities.

Table 3 The calculated IR and Raman spectral data for the studied CN polymorphs (blank corresponds to zero intensity)

		ν, cm^{-1}		IR, D^2 Å^{-2} amu^{-1}		Raman, Å^4	
Mode	Symmetry	**NCNC**	**NCCN**	**NCNC**	**NCCN**	**NCNC**	**NCCN**
1	e	375.1	431.7	10.6		93.3	2.8
2	e	375.1	431.7	10.6		93.4	2.9
3	a_1	440.4	549.0	3.4		854.7	9.1
4	a_1	784.2	1051.6	3.7	1.1	108.2	0.1
5	a_1	961.9	1113.2	92.4		198.2	66.3
6	e	1008.9	1180.9	50.3	12.0	20.1	
7	e	1008.9	1180.9	50.3	12.0	20.2	0.1
8	e	1223.3	1197.1	418.6		9.5	44.0
9	e	1223.3	1197.1	418.6		9.5	44.0

In contrast, the **NCNC** phase demonstrates a more informative spectrum. The valence vibrations of the *e* symmetry at 1223.3 cm^{-1} have a rather high intensity (418.6 D^2 $Å^{-2}$ amu^{-1}) and can be detected experimentally. A graphical description of the vibrational modes is illustrated in Fig. S2 in the ESI.† A similar behavior is observed in the case of their Raman activities (Table 3). The **NCCN** phase demonstrates two relatively active vibrations for the a_1 and *e* symmetry at 1113.2 cm^{-1} (66.3 A^4) and 1197.1 cm^{-1} (44.0 A^4), respectively. Meanwhile, the **NCNC** polymorph has three much more active a_1 symmetry bands at 440.4 cm^{-1} (854.7 A^4), 784.2 cm^{-1} (108.2 A^4) and 961.9 cm^{-1} (198.2 A^4).

To gain more information for spectral identification of the presented carbon nitride phases, we studied their optical properties based on the calculation of the complex dielectric function $\varepsilon(\omega) = \varepsilon_1(\omega) + i\varepsilon_2(\omega)$. The electronic transition between the valence and conducting bands in a solid is described by the imaginary part of this function (eqn (2))[69]

$$\varepsilon_2(\omega) = \frac{1}{4\pi\varepsilon_0}\left(\frac{2\pi e}{m\omega}\right)^2 \sum_{k,c,v} \left|\langle \psi_k^c | ep | \psi_k^v \rangle\right|^2 \delta\left(E_k^c - E_k^v - \hbar\omega\right) \quad (2)$$

where *c* and *v* specify the conducting and valence band states, respectively. To obtain the real part $\varepsilon_1(\omega)$ of the dielectric function, one can apply the Kramers–Kronig transformation (eqn (3)).[69]

$$\varepsilon_1(\omega) = 1 + \left(\frac{2}{\pi}\right)\int_0^\infty d\omega' \frac{\omega'^2 \varepsilon_2(\omega')^2}{\omega'^2 - \omega^2} \quad (3)$$

Subsequently, the absorption coefficient (α) can be expressed as follows (eqn (4)).[69] Note, the plots of the other derivative optical properties, namely, reflectivity, refractive index, conductivity and loss function together with the corresponding equations are illustrated in Fig. S3 and S4 in the ESI.†

$$\alpha(\omega) = \sqrt{2}\left[\sqrt{\varepsilon_1^2(\omega) + \varepsilon_2^2(\omega)} - \varepsilon_1(\omega)\right]^{1/2} \quad (4)$$

Thus, the calculated absorption spectra of the **NCNC** and **NCCN** polymorphs are illustrated in Fig. 4, which were obtained using the highly accurate NCP/HSE06/700 eV approach. Although, the calculations were performed for three directions of polarized incident light, the [1 0 0] and [0 1 0] directions are identical due to the symmetry constraints. The positions of λ_{max} were distinguished using a plot of $\partial^2\varepsilon/\partial E^2$ *vs.* *E*. The obtained absorption spectra are in good accordance with the BS calculations (Fig. 2). The lowest energy band lies at *ca.* 200 nm (**NCNC**) and 155 nm (**NCCN**). These bands do not correspond to the transitions from the valence band maximum (VBM) to the conduction band minimum (CBM), whereas the VBM → CBM transition is higher in energy. The spectrum of the **NCCN** phase is characterized by a similar absorption pattern in both symmetry nonequivalent directions (Fig. 4). In contrast, in the case of the **NCNC** polymorph, two strong absorption peaks appear at 108 and 132 nm in the [0 0 1] direction. Generally, the strongest absorption is expected to be at about 70 nm in both cases. Thus, similarly to the previously predicted trigonal nitrogen allotrope,[2] the discussed carbon nitrides are expected to be transparent to visible light as well as to A and B ultraviolet light.

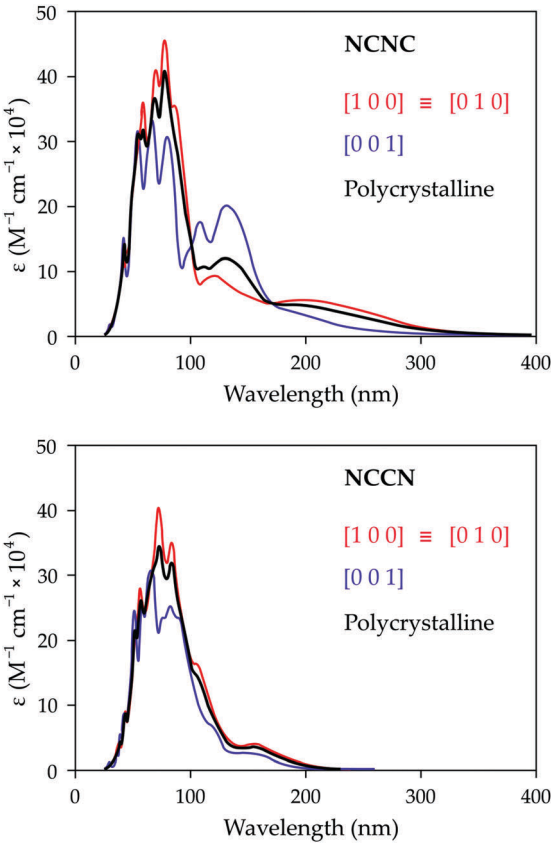

Fig. 4 Calculated absorption spectra of the studied CN polymorphs using the NCP/HSE06/700 eV approach.

In addition to the vibrational and electronic spectra, we calculated the nuclear magnetic resonance (NMR) properties of both phases using the gauge-including projector augmented-wave method (GIPAW)[70] and electric field gradient (EFG) values. The detection of nuclear quadrupole resonance (NQR) parameters in carbon nitrides is based on the NQR-active isotopes ^{14}N and ^{14}C which have $I > 1/2$. The calculated results are presented in Table 4.

According to Table 4, we used the absolute values of magnetic shielding tensor (σ_{iso}) since the choice of NMR reference in theoretical calculations may become critical.[71] In contrast to the recently predicted trigonal nitrogen allotrope[2] and 2D nitrogen[72] or polyguanidine sheets,[73] the σ_{iso} values at the nitrogen atoms are positive and are shifted towards a stronger field, which assume a much denser electron arrangement. The **NCNC** and **NCCN** polymorphs demonstrate rather different quadrupole coupling constant values (C_Q). In the latter case these constants are all negative, which suggests that the nuclei have an oblate spheroid shape along the spin axis. In the case of the **NCNC** phase the two inner atoms, C2 and N3, display positive C_Q constant values (Table 4), which assume a prolate spheroid shape of the nuclei.

Table 4 Chemical shielding and electric field gradient (EFG) tensors at the symmetry unique atoms in the studied carbon nitride phases

Atom	Shielding tensor			EFG tensor	
	σ_{iso}[a] (ppm)	Δ[b] (ppm)	η[c]	C_Q[d] (MHz)	η_Q[e]
NCNC					
N1	125.75	91.15	0.06	−6.03	0.00
C2	81.36	15.15	0.35	1.47	0.00
N3	139.45	5.01	0.84	8.26	0.00
C4	46.07	84.97	0.06	−6.34	0.00
NCCN					
N1	139.55	58.34	0.09	−5.67	0.00
C2	90.17	−6.17	0.81	−1.35	0.00
C3	90.17	−6.17	0.81	−1.35	0.00
N4	139.55	58.34	0.09	−5.67	0.00

[a] $\sigma_{iso} = (\sigma_{xx} + \sigma_{yy} + \sigma_{zz})/3$. [b] $\Delta = \sigma_{zz} - \sigma_{iso}$. [c] $\eta = (\sigma_{xx} - \sigma_{yy})/\Delta$. [d] $C_Q = eQV_{zz}/h$, where, V_{zz} is the largest component of the diagonalized EFG tensor, Q is the nuclear quadrupole moment and h is Plank's constant. [e] $\eta Q = (V_{xx} - V_{yy})/V_{zz}$.

Mechanical and thermodynamic properties

In our comprehensive study of the **NCNC** and **NCCN** carbon nitride polymorphs we estimated their mechanical robustness. The latter is based on the corresponding elastic constants calculation. Thus, we obtained the values of elastic stiffness (C_{ij}) and compliance (S_{ij}) constants which are listed in Tables S1 and S2 in the ESI.† For an appropriate mechanical stability, the independent elastic constants of a crystal should satisfy the corresponding Born–Huang criteria. In the case of the hexagonal Bravais lattice of the Laue class $\bar{3}m$, there are 6 independent elastic constants, and thus, four necessary and sufficient criteria (eqn (5)).[74]

$$\begin{cases} C_{11} > |C_{12}|; C_{44} > 0; \\ C_{13}^2 < 1/2C_{33}(C_{11} + C_{12}); \\ C_{14}^2 < 1/2C_{44}(C_{11} - C_{12}) \equiv C_{44}C_{66}. \end{cases} \quad (5)$$

As seen in Table S1 (ESI†), the corresponding independent elastic constants obey all the Born–Huang criteria. Thus, the studied carbon nitrides are mechanically stable. Since **NCNC** and **NCCN** are layered materials, these polymorphs are expected to demonstrate strong mechanical anisotropy, which is consistent with the Young's modulus values in Table 5. Remarkably, along the x and y directions, which form the layer plane, the Young's modulus values are very high. In the case of the **NCNC** phase, its elastic modulus is about 90% that of graphene. The **NCCN** isomer exhibits a slightly lower value, which is about 80% the robustness of graphene. Naturally, in the perpendicular direction z, the values are much lower and thus, easy exfoliation is assumed.

To provide a 3D view of the Young's modulus, we built the corresponding contours on the basis of the elastic compliance constants (S_{ij}) in accordance with eqn (6):[75]

$$\frac{1}{E} = (1 - l_3^2)^2 s_{11} + l_3^4 s_{33} + l_3^2(1 - l_3^2)(2s_{13} + s_{44}) + 2l_2l_3(3l_1^2 - l_2^2)s_{14} \quad (6)$$

Table 5 Young modulus (E, GPa) and Poisson ratios (ν) for the studied carbon nitride polymorphs

Axis	E (GPa)	Poisson ratios (ν)			
NCNC					
x	914.6279	E_{xy}	0.1125	E_{xz}	0.0363
y	914.6279	E_{yx}	0.1125	E_{yz}	0.0363
z	73.2596	E_{zx}	0.0029	E_{zy}	0.0029
NCCN					
x	865.0951	E_{xy}	0.1907	E_{xz}	−0.1397
y	865.0951	E_{yx}	0.1907	E_{yz}	−0.1397
z	58.3925	E_{zx}	−0.0094	E_{zy}	−0.0094

where $l_1 = \sin\theta\cos\varphi$, $l_2 = \sin\theta\sin\varphi$ and $l_3 = \cos\theta$ are the directional sinuses and cosines of angles in the three principal directions. The obtained 3D plots and the three projections on the secant planes are shown in Fig. 5. It should be noted that the axis orientations in Fig. 5 and Table 5 do not match. Generally, the studied carbon nitrides are soft materials with bulk moduli equal to 64.80 GPa and 50.91 GPa for the **NCNC** and **NCCN** polymorphs, respectively. These values are significantly lower than the corresponding bulk moduli for other carbon nitrides.[36,37]

Using the vibrational spectra calculations, we obtained the thermodynamic properties of the studied polymorphs in the temperature range of 0 to 1000 K. Graphically, the temperature dependence of the thermodynamic functions is illustrated in Fig. S5 in the ESI.† Among the thermodynamic functions, we estimated the zero-point vibrational energy (ZPE), enthalpy (H), entropy (S), Gibbs free energy (G), constant pressure heat capacity (C_P) and Debye temperature (Θ_D). The latter can be expressed by eqn (7):

$$\Theta_D = \frac{h}{k_B}\sqrt[3]{\frac{3n}{4\pi}\left(\frac{N_A\rho_{cryst}}{MW}\right)}\nu_m \quad (7)$$

where h is the Planck's constant, k_B is the Boltzmann constant, n is the number of atoms per unit cell, N_A is Avogadro's

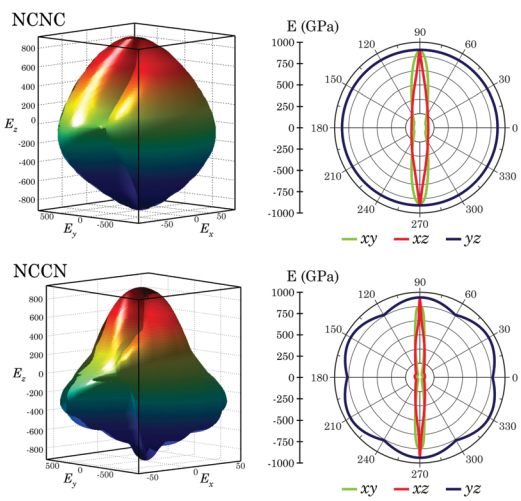

Fig. 5 3D Young's modulus plots of the studied carbon nitride polymorphs together with the three projections on the secant planes.

Table 6 The calculated thermodynamic properties (at 298 K) for the studied carbon nitride polymorphs

Species	ZPE[a,b]	H^b	G^b	S^c	$C_P{}^d$	Θ_D
NCNC	44.69	3.07	−1.35	14.84	27.46	1380[e]
NCCN	50.56	2.23	−0.87	10.40	21.96	1653[f]

[a] Zero point energy. [b] Values in kJ mol^{-1}. [c] Values in J mol^{-1} K^{-1}. [d] Values in J cell^{-1} K^{-1}. [e] Value at 108 K. [f] Value at 151 K.

number, ρ_{cryst} is the crystal density, MW is the molecular weight, and ν_m is the average sound velocity. The numerical values of the obtained thermodynamic properties at 298 K are listed in Table 6.

The **NCNC** and **NCCN** phases have good cohesive energies, which are equal to 7.74 and 8.31 eV atom^{-1}, respectively. These cohesive energy values are stronger than those calculated by Kim *et al.*[33] for six other carbon nitride phases, which vary from 6.30 eV atom^{-1} (for ZB) to 7.69 eV atom^{-1} (for BCT). However, we should stress that the calculated cohesive energy for diamond is equal to 8.07 eV atom^{-1}.[33] In the presented study, we recalculated the energy for diamond, which was found to be equal to 9.17 eV atom^{-1}. Thus, taking into account the absolute underestimation (1.1 eV) by Kim *et al.*,[33] we conclude that the **NCCN** phase is stronger than all the reported polymorphs except BCT. In contrast, the **NCNC** phase is slightly weaker than both the BCT and tet-RS polymorphs.[33]

QTAIM analysis of the interlayer interactions

Analysis of the scalar field in real space in terms of Quantum Theory of Atoms in Molecules (QTAIM) was performed to study the interlayer interactions. Thus, a number of symmetry-unique critical points (CPs) were found in the interlayer space. In the case of weak interactions (intermolecular, hydrogen bonding, *etc.*), the values of the potential energy density $\nu(\mathbf{r})$ at BCPs can be applied as a measure of strength of the corresponding weak bonds in accordance with the Espinosa equation (eqn (8)):[76]

$$E = 1312.75\nu(\mathbf{r}),\ \text{kJ mol}^{-1} \quad (8)$$

The quantity $\nu(\mathbf{r})$ can be obtained using $\rho(\mathbf{r})$ and its Laplacian $\nabla^2\rho(\mathbf{r})$ in terms of the Abramov's gradient expansion (eqn (9)).[77]

$$\nu(\mathbf{r}) = -\frac{3}{5}\left(3\pi^2\right)^{2/3}\rho(\mathbf{r})^{5/3} - \frac{1}{12}\nabla^2\rho(\mathbf{r}) \quad (9)$$

It is also known that $\nabla^2\rho(\mathbf{r})$ is usually utilized to discriminate covalent bonds and closed-shell interactions.[78] Negative values of $\nabla^2\rho(\mathbf{r})$ are characteristic of covalent bonds. Thus, we separated the BCPs, which correspond to weak interlayer interactions. The obtained symmetry-unique BCPs for the studied carbon nitrides and graphite, as a reference, are presented in Table 7. A complete list of the CPs together with their fractional coordinates is presented in Tables S3–S5 (ESI†) and the arrangement of the CPs inside the asymmetric cells is presented in Fig. S6 in the ESI.†

The absence of negative values of $\nabla^2\rho(\mathbf{r})$ suggests that all the interlayer BCPs correspond to closed-shell interactions (Table 7). Thus, the estimated interlayer interaction energies calculated using eqn (8) are as follows: 15.69 (**NCNC**), 11.22 (**NCCN**) and 5.92 kJ mol^{-1} (graphite). We should stress that these values correlate well (R^2 = 0.996) with the bulk moduli of the studied carbon nitrides and the calculated value of graphite (30.0 GPa). Thus, it is obvious that the studied carbon nitrides can be relatively easily exfoliated, and their applied energies are approximately 2–3 times higher than that of graphite.

Table 7 The calculated QTAIM parameters (kJ mol^{-1}) at the BCPs between the layers

Entry	Symm.	Mult.	$\rho(\mathbf{r})$	$\nabla^2\rho(\mathbf{r})$	$\nu(\mathbf{r})$
NCNC	C_S	3	10.89	32.03	−5.23
NCCN	C_{2h}	3	8.92	22.82	−3.74
Graphite	D_{3d}	2	7.04	20.62	−2.96

Conclusions

In summary, we have presented a comprehensive study of two isomeric layered carbon nitride polymorphs. The two studied phases demonstrate strong mechanical anisotropy, but due to their layered structure, their corresponding bulk moduli are dramatically lower in comparison with the previously obtained polymorphs. Their exfoliation energies are relatively small, which enables the use of the **NCNC** and **NCCN** phases for coating processes. Similarly to the recently reported 2D boron nitrides,[79] the obtained coatings are expected to be very resistant to impact. This outlines the perspectives for the further study of 2D materials on the basis of the **NCNC** and **NCCN** polymorphs. Our preliminary calculations suggest that these 2D materials possess dynamic and mechanical stability.

Due to the different natures of their surfaces, the 2D monolayers of the **NCNC** and **NCCN** carbon nitrides are expected to have different waterproofing properties. This assumption is based on our preliminary calculations of adsorption energies of a water molecule. It is worthwhile to note that in the case of **NCNC**, adsorption is more exothermic than for **NCCN** and the energy is almost the same for both sides of the **NCNC** layer. Depending on the nature of the substrate, the 2D **NCNC** carbon nitride can be grafted by different atomic edges. Thus, a surface with both nitrogen and carbon atoms on top can be obtained. Finally, it is interesting to track the evolution of band structure from a layered phase towards a purely two-dimensional phase, which can reveal interesting electronic properties for the obtained 2D materials. From this point of view, 3D and 2D forms of the studied carbon nitrides have potential application in the field of solar energy conversion or photonics as wide band gap semiconductors.[80]

Conflicts of interest

There are no conflicts to declare.

Acknowledgements

This study was supported by the Ministry of Education and Science of Ukraine, Research Fund (Grant No. 0113U001694).

We thank Professor Hans Ågren (KTH, Stockholm) for the PDC supercomputer use. The computations were performed on resources provided by the Swedish National Infrastructure for Computing (SNIC) at the Parallel Computer Center (PDC) through the project ''Multiphysics Modeling of Molecular Materials'', SNIC 020/11-23.

Notes and references

1 M. I. Eremets, A. G. Gavriliuk, I. A. Trojan, D. A. Dzivenko and R. Boehler, *Nat. Mater.*, 2004, **3**, 558–563.
2 S. V. Bondarchuk and B. F. Minaev, *Phys. Chem. Chem. Phys.*, 2017, **19**, 6698–6706.
3 D. Hanlon, C. Backes, E. Doherty, C. S. Cucinotta, N. C. Berner, C. Boland, K. Lee, A. Harvey, P. Lynch, Z. Gholamvand, S. Zhang, K. Wang, G. Moynihan, A. Pokle, Q. M. Ramasse, N. McEvoy, W. J. Blau, J. Wang, G. Abellan, F. Hauke, A. Hirsch, S. Sanvito, D. D. O'Regan, G. S. Duesberg, V. Nicolosi and J. N. Coleman, *Nat. Commun.*, 2015, **6**, 8563.
4 H. Sun, Y. Cao, L. Feng and Y. Chen, *Sci. Rep.*, 2016, **6**, 22808.
5 Y. Wu, S. Chen, J. Zhao, X. Yue, W. Deng, Y. Li and C. Wang, *J. Environ. Chem. Eng.*, 2016, **4**, 797–807.
6 M. Xiong, L. Chen, Q. Yuan, J. He, S.-L. Luo, C.-T. Au and S.-F. Yin, *Carbon*, 2015, **86**, 217–224.
7 H. Li, Y. Liu, X. Gao, C. Fu and X. Wang, *ChemSusChem*, 2015, **8**, 1189–1196.
8 M. Shalom, S. Inal, D. Neher and M. Antonietti, *Catal. Today*, 2014, **225**, 185–190.
9 J. Wirth, R. Neumann, M. Antonietti and P. Saalfrank, *Phys. Chem. Chem. Phys.*, 2014, **16**, 15917–15926.
10 H. Zhang, X. Zuo, H. Tang, G. Li and Z. Zhou, *Phys. Chem. Chem. Phys.*, 2015, **17**, 6280–6288.
11 K. Qiu and Z. Xiao Guo, *J. Mater. Chem. A*, 2014, **2**, 3209–3215.
12 X. Fu, X. Hu, Z. Yan, K. Lei, F. Li, F. Cheng and J. Chen, *Chem. Commun.*, 2016, 1725–1728.
13 Y. Qin, J. Li, J. Yuan, Y. Kong, Y. Tao, F. Lin and S. Li, *J. Power Sources*, 2014, **272**, 696–702.
14 C. Hu, Q. Han, F. Zhao, Z. Yuan, N. Chen and L. Qu, *Sci. China Mater.*, 2015, **58**, 21–27.
15 J.-M. Fan, J.-J. Chen, Q. Zhang, B.-B. Chen, J. Zang, M.-S. Zheng and Q.-F. Dong, *ChemSusChem*, 2015, **8**, 1856–1861.
16 H. Pan, *J. Phys. Chem. C*, 2014, **118**, 9318–9323.
17 G. Koh, Y.-W. Zhang and H. Pan, *Int. J. Hydrogen Energy*, 2012, **37**, 4170–4178.
18 M. Bezi Javan, M. D. Ganji, M. Sabet and N. Danesh, *J. Comput. Theor. Nanosci.*, 2011, **8**, 803–807.
19 M. Amiri, H. Salehniya and A. Habibi-Yangjeh, *Ind. Eng. Chem. Res.*, 2016, **55**, 8114–8122.
20 A. Du, S. Sanvito and S. C. Smith, *Phys. Rev. Lett.*, 2012, **108**, 197207.
21 A. Y. Liu and M. L. Cohen, *Science*, 1989, **245**, 841–842.
22 D. M. Teter and R. J. Hemley, *Science*, 1996, **271**, 53–55.
23 A. Reyes-Serrato, D. H. Galvan and I. L. Garzon, *Phys. Rev. B: Condens. Matter Mater. Phys.*, 1995, **52**, 6293–6300.
24 G.-M. Rignanese, J.-C. Charlier and X. Gonze, *Phys. Rev. B: Condens. Matter Mater. Phys.*, 2002, **66**, 205416.
25 A. Y. Liu and R. M. Wentzcovitch, *Phys. Rev. B: Condens. Matter Mater. Phys.*, 1994, **50**, 10362(R).
26 I. Alves, G. Demazeau, B. Tanguy and F. Weill, *Solid State Commun.*, 1999, **109**, 697–701.
27 J. E. Lowther, *Phys. Rev. B: Condens. Matter Mater. Phys.*, 1998, **57**, 5724–5727.
28 H. Wang, X. Jiang, S. Yin, D. Li and D. Liu, *RSC Adv.*, 2015, **5**, 70682–70688.
29 J. V. Badding and D. C. Nesting, *Chem. Mater.*, 1996, **8**, 535–540.
30 M. Côté and M. L. Cohen, *Phys. Rev. B: Condens. Matter Mater. Phys.*, 1997, **55**, 5684–5688.
31 M. Khazaei, M. Nath Tripathi and Y. Kawazoe, *Phys. Rev. B: Condens. Matter Mater. Phys.*, 2011, **83**, 134111.
32 X. Wang, *J. Chem. Phys.*, 2012, **137**, 184506.
33 E. Kim, C. F. Chen, T. Kohler and M. Elstner, *Phys. Rev. Lett.*, 2001, **86**, 652–655.
34 X. Wang, K. Bao, F. Tian, X. Meng, C. Chen, B. Dong, D. Li, B. Liu and T. Cui, *J. Chem. Phys.*, 2010, **133**, 044512.
35 J. N. Hart, F. Claeyssens, N. L. Allan and P. W. May, *Phys. Rev. B: Condens. Matter Mater. Phys.*, 2009, **80**, 174111.
36 M. Zhang, Q. Wei, H. Yan, Y. Zhao and H. Wang, *J. Phys. Chem. C*, 2014, **118**, 3202–3208.
37 E. Stavrou, S. Lobanov, H. Dong, A. R. Oganov, V. B. Prakapenka, Z. Konôpková and A. F. Goncharov, *Chem. Mater.*, 2016, **28**, 6925–6933.
38 N. Li, W. Xuan-Zhang, Z. Jia-Qi and G. Wei, *Chin. Phys. B*, 2013, **22**, 017101.
39 J. T. Titantah and D. Lamoen, *Phys. Status Solidi A*, 2006, **203**, 3191–3197.
40 G. K. Gueorguiev, J. Neidhardt, S. Stafström and L. Hultman, *Chem. Phys. Lett.*, 2005, **401**, 288–295.
41 G. K. Gueorguiev, J. Neidhardt, S. Stafström and L. Hultman, *Chem. Phys. Lett.*, 2005, **410**, 228–234.
42 L. Hultman, S. Stafström, Z. Czigány, J. Neidhardt, N. Hellgren, I. F. Brunell, K. Suenaga and C. Colliex, *Phys. Rev. Lett.*, 2001, **87**, 225503.
43 S. Jalili, F. Molani and J. Schofield, *J. Theor. Comput. Chem.*, 2014, **13**, 1450021.
44 H. Pan, Y.-W. Zhang, V. B. Shenoy and H. Gao, *Nanoscale Res. Lett.*, 2011, **6**, 97.
45 G. Chai, C. Lin, M. Zhang, J. Wang and W. Cheng, *J. Nanotechnol.*, 2010, **21**, 195702.
46 J. Gracia and P. Kroll, *J. Mater. Chem.*, 2009, **19**, 3020–3026.
47 A. Nazrul Rosli, N. Ahmad Zabidi, H. A. Kassim and K. N. Shrivastava, *J. Cluster Sci.*, 2010, **21**, 197–210.
48 M. M. Al Mogren, A. A. El-Azhary, W. Z. Alkiali and M. Hochlaf, *J. Phys. Chem. A*, 2010, **114**, 12258–12268.
49 H. Qiu, Z. Wang and X. Sheng, *Phys. Lett. A*, 2013, **377**, 347–350.
50 A. Hu and F. Zhang, *J. Phys.: Condens. Matter*, 2010, **22**, 505402.

51 S. J. Clark, M. D. Segall, C. J. Pickard, P. J. Hasnip, M. J. Probert, K. Refson and M. C. Payne, *Z. Kristallogr.*, 2005, **220**, 567–570.

52 *Materials Studio 7.0*, Accelrys, Inc., San Diego, CA, 2013.

53 J. P. Perdew, K. Burke and M. Ernzerhof, *Phys. Rev. Lett.*, 1996, **77**, 3865.

54 J. P. Perdew, A. Ruzsinszky, G. I. Csonka, O. A. Vydrov, G. E. Scuseria, L. A. Constantin, X. Zhou and K. Burke, *Phys. Rev. Lett.*, 2008, **100**, 136406.

55 J. P. Perdew, J. A. Chevary, S. H. Vosko, K. A. Jackson, M. R. Pederson, D. J. Singh and C. Fiolhais, *Phys. Rev. B: Condens. Matter Mater. Phys.*, 1992, **46**, 6671–6687.

56 C. Adamo and V. Barone, *J. Chem. Phys.*, 1998, **110**, 6158–6170.

57 A. D. Becke, *J. Chem. Phys.*, 1993, **98**, 5648–5652.

58 J. Heyd and G. Scuseria, *J. Chem. Phys.*, 2004, **121**, 1187–1192.

59 G. M. Dongho Nguimdoa and D. P. Joubert, *Eur. Phys. J. B*, 2015, **88**, 113.

60 A. Tkatchenko and M. Scheffler, *Phys. Rev. Lett.*, 2009, **102**, 073005.

61 F. Ortmann, F. Bechstedt and W. G. Schmidt, *Phys. Rev. B: Condens. Matter Mater. Phys.*, 2006, **73**, 205101.

62 S. V. Bondarchuk and B. F. Minaev, *RSC Adv.*, 2015, **5**, 11558–11569.

63 J. A. Alarco, A. Chou, P. C. Talbota and I. D. R. Mackinnon, *Phys. Chem. Chem. Phys.*, 2014, **16**, 24443–24456.

64 Virtual NanoLab 2016.3, QuantumWise A/S, www.quantumwise.com.

65 A. Otero-De-La-Roza, E. R. Johnson and V. Luaña, *Comput. Phys. Commun.*, 2014, **185**, 1007–1018.

66 G. Kresse and D. Joubert, *Phys. Rev. B: Condens. Matter Mater. Phys.*, 1999, **59**, 1758.

67 P. Giannozzi, S. Baroni, N. Bonini, M. Calandra, R. Car, C. Cavazzoni, D. Ceresoli, G. L. Chiarotti, M. Cococcioni, I. Dabo, A. Dal Corso, S. Fabris, G. Fratesi, S. de Gironcoli, R. Gebauer, U. Gerstmann, C. Gougoussis, A. Kokalj, M. Lazzeri, L. Martin-Samos, N. Marzari, F. Mauri, R. Mazzarello, S. Paolini, A. Pasquarello, L. Paulatto, C. Sbraccia, S. Scandolo, G. Sclauzero, A. P. Seitsonen, A. Smogunov, P. Umari and R. M. Wentzcovitch, *J. Phys.: Condens. Matter*, 2009, **21**, 395502.

68 W. Setyawan and S. Curtarolo, *Comput. Mater. Sci.*, 2010, **49**, 299–312.

69 M. Sheik-Bahae, Nonlinear Optics Basics. Kramers-Kronig Relations in Nonlinear Optics. in *Encyclopedia of Modern Optics*, ed. R. D. Guenther, Academic Press, Amsterdam, 2005, pp. 234–239.

70 C. J. Pickard and F. Mauri, *Phys. Rev. B: Condens. Matter Mater. Phys.*, 2001, **63**, 245101.

71 M. Dračínský, M. Šála, B. Klepetářová, J. Šebera, J. Fukal, V. Holečková, Y. Tanaka, R. Nencka and V. Sychrovský, *J. Phys. Chem. B*, 2016, **120**, 915–925.

72 S. V. Bondarchuk and B. F. Minaev, *Comput. Mater. Sci.*, 2017, **133**, 122–129.

73 S. V. Bondarchuk and B. F. Minaev, *Mol. Phys.*, 2017, **115**, 2423–2430.

74 F. Mouhat and F.-X. Coudert, *Phys. Rev. B: Condens. Matter Mater. Phys.*, 2014, **90**, 224104.

75 J. F. Nye, *Physical properties of crystals*, Oxford University Press Inc., Oxford, 1985.

76 E. Espinosa, E. Molins and C. Lecomte, *Chem. Phys. Lett.*, 1998, **285**, 170–173.

77 Yu. A. Abramov, *Acta Crystallogr.*, 1997, **A53**, 264–272.

78 R. F. W. Bader, *Atoms in Molecules. A Quantum Theory*, Oxford University Press, Oxford, 1990.

79 N. N. Karaush, S. V. Bondarchuk, G. V. Baryshnikov, V. A. Minaeva, W.-H. Sun and B. F. Minaev, *RSC Adv.*, 2016, **6**, 49505–49516.

80 D. Klimm, *IUCrJ*, 2014, **1**, 281–290.

